Brain aerobic glycolysis and motor adaptation learning

Benjamin J. Shannon[a,1], Sanjeev Neil Vaishnavi[a,b,1], Andrei G. Vlassenko[a], Joshua S. Shimony[a], Jerrel Rutlin[a], and Marcus E. Raichle[a,c,d,e,2]

[a]Mallinckrodt Institute of Radiology, Washington University in St. Louis, St. Louis, MO 63110; [b]Department of Neurology, University of Pennsylvania, Philadelphia, PA 19104; [c]Department of Neurology, Washington University in St. Louis, St. Louis, MO 63110; [d]Department of Biomedical Engineering, Washington University in St. Louis, St. Louis, MO 63110; and [e]Department of Anatomy and Neurobiology, Washington University in St. Louis, St. Louis, MO 63110

Ten percent to 15% of glucose used by the brain is metabolized nonoxidatively despite adequate tissue oxygenation, a process termed aerobic glycolysis (AG). Because of the known role of glycolysis in biosynthesis, we tested whether learning-induced synaptic plasticity would lead to regionally appropriate, learning-dependent changes in AG. Functional MRI (fMRI) before, during, and after performance of a visual–motor adaptation task demonstrated that left Brodmann area 44 (BA44) played a key role in adaptation, with learning-related changes to activity during the task and altered resting-state, functional connectivity after the task. PET scans before and after task performance indicated a sustained increase in AG in left BA 44 accompanied by decreased oxygen consumption. Intersubject variability in behavioral adaptation rate correlated strongly with changes in AG in this region, as well as functional connectivity, which is consistent with a role for AG in synaptic plasticity.

aerobic glycolysis | long-term potentiation | learning | long-term depression | PET

The resting brain's energy needs are supported almost entirely by the metabolism of glucose to carbon dioxide and water (1). The first step of this process, glycolysis, requires no oxygen whereas the second step, oxidative phosphorylation, does. In the normal adult human brain, 10–15% of the glucose never reaches the second step—it is shunted away from oxidative phosphorylation despite the presence of adequate oxygen (2–5). This process is commonly referred to as aerobic glycolysis (AG).

Several roles for AG have been identified, including biosynthesis (for recent reviews, see refs. 6–8), the regulation of cellular redox states (9, 10), the regulation of apoptosis (11), the provision of ATP for membrane pumps (12–14), and the regulation of cell excitability (15, 16). More recently, similar functions of AG have been observed in the posttranscriptional control of T-cell effector function (17, 18), an observation now extended to the microglia (19), where it is associated with an activated state related to inflammation as well as synaptic pruning.

In the developing human brain, at a time when synaptic growth rates are highest (approximately age 10), total glucose consumption is twice that of the adult, and 30% of that glucose consumption is AG (a recent summary of this early literature is contained in ref. 20), suggesting an important role in brain development. Another remarkable feature of AG in the adult human brain is that it varies regionally (21): nearly 25% of resting glucose consumption in the medial prefrontal cortex is AG whereas AG constitutes as little as 2% glucose consumption in the cerebellum and medial temporal lobes. Correlation of these regional data with regional gene expression in the adult human brain revealed increased gene expression typical of infancy (i.e., neotony) that is related to synapse formation and growth (20).

Further supporting the link between AG and plasticity are findings demonstrating that lactate, released by astrocytes and taken up by neurons, is critical for memory formation. Neuronal uptake of lactate changes the intracellular redox balance in such a way that glycolytic intermediates are shifted away from oxidative phosphorylation and into biosynthetic roles (for a review, see ref. 22). Blockade of astrocyte-produced lactate (23, 24) disrupted memory formation

in rats performing a spatial memory task. Infusion of lactate into the hippocampus improved memory performance (23) and promoted expression of plasticity-related genes (25).

The only direct, human in vivo test of the hypothesis that AG may support learning-associated synaptic plasticity comes from the work of Madsen et al. (26). In their research, they used the classic Kety–Schmidt technique for the quantitative measurement of whole brain blood flow and metabolism (27), before, during, and after the performance of a challenging cognitive task [the Wisconsin Card Sorting Test (28–30), which exhibits a significant learning component (31–33)]. During task performance, they observed an increase in whole brain blood flow, glucose consumption, and lactate production, but no increase in oxygen consumption. Thus, as expected (34–36), the task-induced increase in glucose consumption represented a net increase in AG. After completion of the task, blood flow and lactate production returned to control values, but glucose consumption (i.e., AG) remained elevated until the experiment was terminated 40 min after completion of the task.

Several observations are noteworthy in the work of Madsen et al. (26). During task, the parallel increase of blood flow, glucose use, and lactate production, in the absence of a change in oxygen consumption, are expected and consistent with prior work (reviewed in ref. 37; see also refs. 5 and 35) and also consistent with views positing a cooperative relationship between astrocytes and neurons driven by the need to recycle glutamate

Significance

A substantial fraction of glucose used by the brain does not enter the oxidative phosphorylation pathway despite the presence of adequate oxygen, a phenomenon known as aerobic glycolysis. Among its several functions, aerobic glycolysis makes substantial contributions to biosynthesis, thus becoming a marker of synaptic plasticity. Combining PET and MRI brain-imaging techniques, we characterized the role of aerobic glycolysis in plasticity during the performance of a motor adaptation learning task. Our findings support a link between aerobic glycolysis and learning as well as providing unexpected evidence of a potential role of microglia in long-term depression and synaptic pruning.

(38). However, the persistence of glucose use after task performance was unexpected, as was the dissociation of glycolysis from both lactate production and blood flow. Importantly, the regional specificity of these findings (26) is unknown because the measurement technique (39) reflects whole-brain metabolism.

Our objective was to explore the regional specificity of these metabolic observations (26) and to determine their relationship to task-induced activations as well as to potential changes in pre- vs. posttask resting-state functional connectivity. Specifically, we set out to test whether performance of a motor adaptation task and attendant synaptic plasticity would alter posttask regional AG in a manner consistent with task-induced synaptic plasticity.

The classic "prism adaptation" experiment (ref. 40, pp. 61–62) exemplifies our motor adaptation paradigm: Well-learned sensory–motor transformations are perturbed, generating large errors on a motor task. After a relatively short period of practice, a process of spatial realignment takes place and reduces errors to near baseline (41). Underlying learning and adaptation is synaptic plasticity (42, 43). Experience-dependent plasticity frequently induces the synthesis of new synaptic components, as well as the remodeling and removal of existing components. We posited that these changes would be associated with task-specific regional changes in glycolysis after the adaptation experience.

We used a multimodal strategy, including PET, task-based functional MRI (fMRI), and resting-state functional connectivity fMRI (fcMRI) to investigate the functional and metabolic effects of regional synaptic plasticity in the human brain.

Results

Subjects. Forty-six healthy, right-handed, neurologically normal participants were recruited from the Washington University community (24 women; mean age for all subjects was 24.4 y). Data from the PET experiments come from a subgroup of 18 subjects. These subjects were scanned using PET before and after performing the motor adaptation task. No fMRI data were obtained on these subjects.

The remaining 28 subjects did not participate in PET scans. We scanned these subjects using fMRI during task performance and also obtained resting-state fMRI scans before and after task. To follow-up on the results from these initial experiments, we further analyzed diffusion tensor imaging (DTI) data from 30 healthy young adults, previously published in Siegel et al. (44).

Overview. We asked subjects to perform an out-and-back reaching task using an MR-compatible stylus and tablet and a visual display screen. In one-half of the subjects, we covertly and gradually imposed a rotation on the mapping between the stylus and the display screen. Because subjects were unaware of this rotation (45), this paradigm allowed us to study neural correlates of motor adaptation without contamination from conscious strategic adjustments to motor performance (46). We acquired blood oxygen level-dependent (BOLD) fMRI during task performance, as well as at rest before and after the task. We obtained PET measurements of blood flow and glucose and oxygen consumption and, from the latter two, computed AG (see *Methods* for details) before and after task performance. Both PET and fMRI results indicated that a region in left Brodmann area 44 (BA44) played an important role in motor adaptation. Activity within the region during task performance was strongly affected by both learning and covert rotation. BA44 showed reductions in resting-state functional connectivity with V1 after task performance on the rotation arm of the study. The magnitude of these reductions was stronger in subjects who made larger errors during the task. DTI results indicated that these two regions were connected by a single, direct, white-matter bundle. BA44 exhibited both an increased AG and decreased oxygen consumption after task performance in the rotation group. Significant metabolic changes in the opposite direction occurred in the control group.

Task Performance. Subjects performed an out-and-back reaching task using an MR-compatible tablet and stylus (Fig. 1 *A* and *B*). Stylus movements were projected to a screen visible to the subjects. In each trial, a center circle was projected to the screen, along with eight equally spaced peripheral circles. One of the peripheral circles would flash, and subjects would move the stylus to that circle and back to the center.

Task accuracy was assessed for each out-and-back movement by calculating peak-speed directional error. We identified the
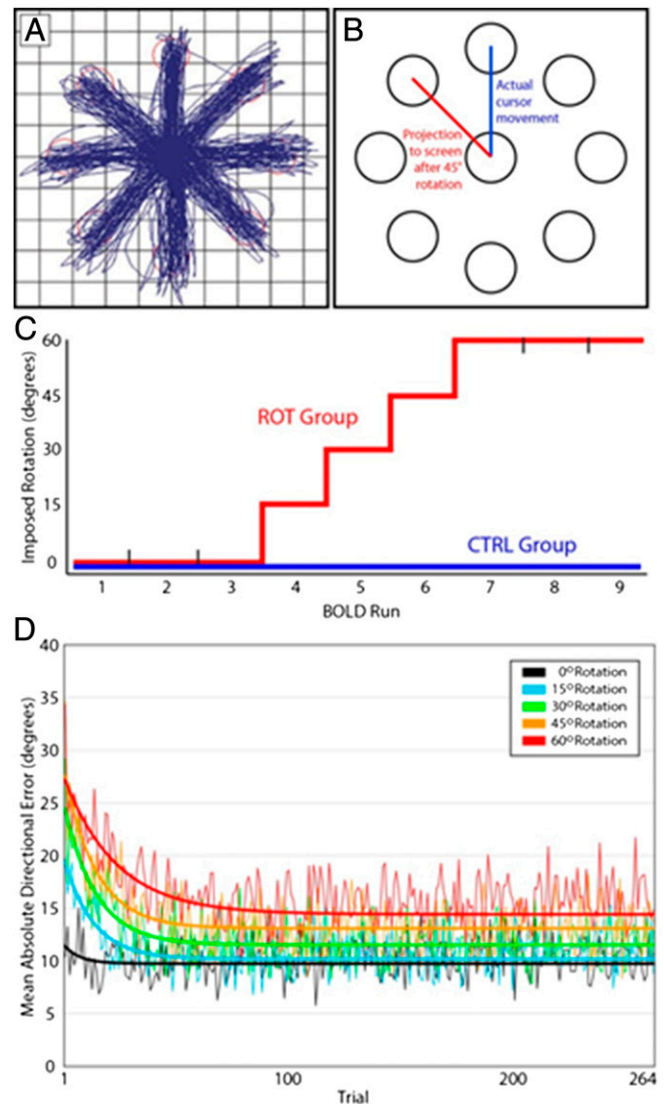

Fig. 1. Task and performance. (*A*) Subjects made out-and-back movements between a central circle and eight peripheral circles. Thin blue lines represent one subject's movements over the course of one BOLD run. (*B*) For one group of subjects, a counterclockwise rotation was imposed on the transformation between stylus and the images projected to the screen. This effect is shown for the 45° rotation case. The curved trajectories illustrated in *A* are generated by correction under visual feedback after the initial excursion. (*C*) Rotations of increasing magnitude were imposed over time after an initial period. Subjects were divided into rotation (ROT) and control (CTRL) groups. The ROT group performed three BOLD runs with no rotation. Rotation was then imposed in step-wise 15° increments up to 60°. Rotation was then held at 60° for two final BOLD runs. No rotation was imposed for the CTRL group. (*D*) Behavioral performance adapted to the imposed rotation. Thin lines represent the absolute directional error averaged across all subjects for that trial number and rotation condition. Thick lines represent best-fit exponential curves.

www.manaraa.com

moment at which the stylus was moving with peak speed, and calculated the directional error at that moment (the difference in degrees between the stylus's actual movement and a straight line directly to the target) and defined that as the mean directional error (MDE).

Subjects were divided into two groups, the rotation (ROT) group, and the control (CTRL) group. Both groups performed two runs of task with no imposed rotation (preadaptation runs). Then, for the ROT group, we covertly imposed a rotation between subjects' actual stylus movements and what was projected on the screen. That is, if subjects made a straight up-and-down movement, the projected result would be rotated clockwise. Correction under visual feedback characteristically generated a counterclockwise-curved trajectory (Fig. 1B). Rotation was imposed in 15° increments over the course of the experiment to a maximum of 60° (Fig. 1C). After adaptation to 60°, ROT subjects performed two more runs of task with constant 60° rotation (postadaptation runs). The CTRL group performed the same number of task runs with no imposed rotation.

Subjects adapted their movements to correct for the imposed rotation. Trajectory error (see *Methods* for details) decayed in an approximately exponential manner (Fig. 1D). After an increase in imposed rotation, accuracy improved quickly over early trials, but reached an asymptote after ∼50 trials. The error level when performance reached asymptote systematically increased with increasing rotation; residual error in 60° rotation trials was substantially larger than in 0° rotation trials. Thus, subjects achieved only partial adaptation.

Brain Activity During Task Performance. Using the fMRI data obtained during task performance, we sought to identify the task-related activity that gave rise to the observed changes in brain metabolism after task performance. We first combined data across groups and conditions and identified brain regions with significant fMRI responses ($n = 28$; $Z > 3.0$, cluster >17, Monte Carlo-corrected). Peak foci were located in the visual cortex, right parietal cortex, left premotor/supplementary motor, and left motor cortex, consistent with performance of a visual–motor task (Fig. 2). Notably, this activity included much of the BA44 region identified in the PET data.

Effects of Imposed Rotation on Task-Evoked Activity. To identify brain areas likely contributing to motor adaptation during the task, we searched for regions whose activity evolved differently between the ROT vs. CTRL groups as well as the beginning vs. end of training. Mathematically, we calculated the time × pre/post × group interaction ANOVA of the event-related responses. This ANOVA identified small portions of the left temporo-parietal junction, left lateral temporal lobe, and, most prominently, a large portion of left BA44, extending into BA45 (Fig. 3).

Special Role of BA44. Left BA44 was independently identified in three separate analyses. The overlap between metabolism changes, main effect of task, and changes in activity after imposed rotation is shown in Fig. 3. Time course analysis of task-evoked responses in BA44 revealed a significant task-evoked response in the pre-training condition for both groups. This activity was maintained in the posttraining condition in the ROT group; however, in the CTRL group, post-training activity returned to baseline (Fig. 3D).

Functional Disconnection Between BA44 and V1 After Imposed Rotation. Resting-state fMRI scans were obtained in all subjects before and after task performance. Having identified the changes in glycolysis and task-evoked BOLD responses in BA44 (Fig. 3), we performed exploratory analyses to test whether BA44 also exhibited changes in functional connectivity. Using the BA44 region identified in the PET experiment as a seed, we performed a whole-brain paired *t*
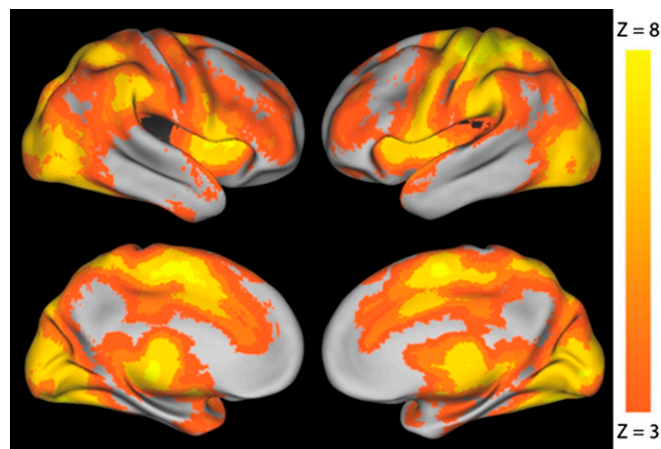

Fig. 2. Regions recruited during task performance. A main-effect-of-task ANOVA indicates brain regions whose functional activity varies as a consequence of task performance. As expected, motor-, vision-, and attention-related regions are recruited. The image is thresholded at $P < 0.01$, multiple-comparison corrected.

test in the ROT group to search for regions whose correlations with BA44 changed after task performance. This procedure identified a single region, in left primary visual cortex (V1), whose correlation with BA44 was reduced (Fig. 4A) ($P < 0.01$; corrected for multiple comparisons). In the ROT group, the two regions were correlated at $r = 0.05$ before the task, which changed to -0.08 after the task. A region comprising contralateral V1 also showed a trend toward a similar reduction, but this contralateral region did not survive multiple comparison correction.

We next performed a post hoc paired *t* test in the CTRL group comparing the BA44:V1 correlation before and after task performance (Fig. 4B). These regions' correlations were not significantly different in the CTRL group. Because the V1 region was defined on the basis of data from the ROT group, we were not able to perform an unbiased comparison of the effect size between groups.

To investigate the spatial specificity of the training effect on BA44:V1 functional connectivity, we defined regions of interest in visual, motor, and parietal regions based on the main-effect-of-task ANOVA. BOLD time series correlations were calculated between each pair of regions, and paired *t* tests were performed to test for changes after training. No other correlations were significantly different after multiple comparisons correction for either the ROT or CTRL group (Fig. 4C). Thus, the training effect on BA44:V1 functional connectivity seems to be spatially specific.

fcMRI Relation to Errors. Covertly imposed rotation, of necessity, induces performance errors. Therefore, mean directional errors (MDEs) in the ROT group were substantially larger than in the CTRL group. Because such errors are critical to motor adaptation, we investigated the relation between performance accuracy and BA44:V1 functional connectivity in each participant (Fig. 5). Although all ROT subjects showed reduced BA44:V1 correlations, some CTRL group subjects with very low error rates actually increased this correlation. Across the CTRL and ROT subjects, we observed a negative correlation: Larger errors were significantly associated with a stronger reduction in BA44:V1 functional connectivity ($r = -0.37$; $P < 0.05$). Crucially, this relationship held even in the CTRL subjects alone ($r = -0.52$; $P < 0.05$), indicating that this effect is not simply a consequence of artificially imposed screen-stylus remapping.

Structural Connections Between BA44 and V1. We tested whether direct white-matter connections existed between our two regions
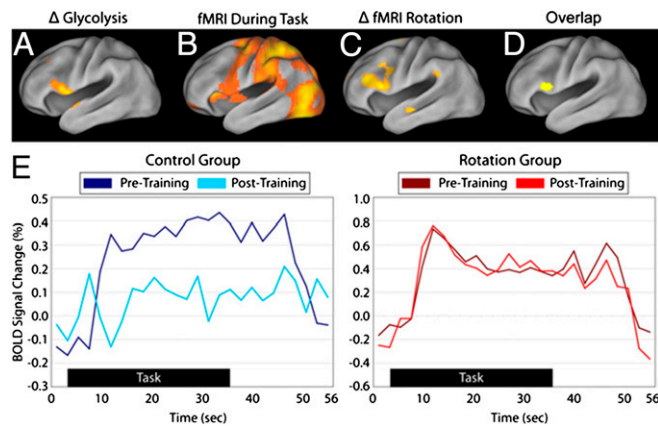
www.manaraa.com

Fig. 3. Brodmann area 44 is closely involved in motor adaptation. (*A*) Increased AG in this area after task performance and imposition of covert rotation. (*B*) Main-effect-of-task ANOVA revealing regions that were recruited during the task. Post hoc *t* tests indicated that all regions in orange increased their activity during task performance. (*C*) Interaction of time-by-task-by-group. This analysis identifies regions whose activity changed between the beginning and the end of the task (runs 1–2 and runs 8–9), and for whom the change differed between ROT and CTRL groups. (*D*) Overlap of *A*, *B*, and *C* reveals a region in left BA44. (*E*) Task-related time courses of activity in BA44 for the CTRL and ROT groups during pre- and posttraining scans.

of interest. We analyzed diffusion tensor imaging (DTI), obtained from a separate group of 30 healthy younger adults (data previously published in ref. 44). Tracts were measured with conventional methods (47), using V1 as the start point and BA44 as the end point. We found that V1 and BA44 are directly connected via robust white-matter tracts (Fig. 6). Tracts were observable in 29 of the 30 subjects.

Error-Evoked Activity. The results presented above show that functional connectivity patterns in the brain change from baseline after task performance. To understand the specific aspects of task performance that contribute to these changes, we measured error-related changes in BOLD activity during the task. We adjusted our task general linear model (GLM) to include the mean directional error (MDE) for each fMRI frame, with a two-frame lag to allow for hemodynamic response delay of the fMRI BOLD signal. This analysis identified regions whose activity correlated with directional error magnitude on a trial-by-trial basis (Fig. 7*A*). The observed correlations were relatively small (averaged over all subjects, the maximum *r* value was 0.037); however, the effects were consistent across subjects, and a random-effects analysis identified several regions whose correlations survived Monte Carlo multiple-comparison correction. The map of error-related activity closely resembled the main-effect-of-task result. Essentially, then, trials with large directional errors recruited similar sets of regions as did task performance as a whole, but with a greater magnitude. Notably, this map includes both BA44 and V1. A hypothesis-driven test of BA44 indicated that it showed increased activity proportional to error magnitude (Fig. 7*B*).

Metabolism. We measured regionally the cerebral blood flow (CBF), the cerebral metabolic rate of oxygen ($CMRO_2$), and the cerebral metabolic rate of glucose (CMRGlu) with PET before and after motor adaptation learning. We tested for regional task-induced changes, with a particular focus on AG, which is measured via the molar ratio of oxygen consumption to glucose utilization. A ratio of 6 indicates that all glucose is metabolized to carbon dioxide and water via oxidative phosphorylation. Importantly, pretask PET scans showed no differences in regional

measurements of metabolism or blood flow between the ROT and CTRL groups (Fig. S1).

We hypothesized that the neural changes underlying motor adaptation would lead to a change in AG in motor-related regions. Thus, we expected to see changes in AG after task performance in the ROT group but not the CTRL group. Statistically, we assessed this hypothesis by performing a whole-brain voxel-wise repeated-measures two-factor ANOVA, with the two factors being task state (pre or post) and group (ROT or CTRL). Resulting maps were converted to equally probable Z-maps and thresholded at $P < 0.0001$ ($n = 18$, $Z > 4.4$, cluster >99 voxels) according to previously described methodology (48, 49). This analysis identified a single region in left BA44 (Fig. 8*A*), which exhibited an increase in AG after task performance in the ROT group and, unexpectedly, a significant reduction in the CTRL group (Fig. 8*B*). We then extracted CBF, $CMRO_2$, and CMRGlu in this region for all subjects and conditions and performed post hoc statistical comparisons. In the ROT group, the increase in AG resulted from both a reduction in oxygen consumption and an increase in glucose utilization (Fig. 8*B*). In the CTRL group, AG was decreased in association with an increase in $CMRO_2$ and CBF when the latter two measures were compared with the ROT group. Our whole-brain regional analyses revealed no other significant effects of motor adaptation on CBF, $CMRO_2$, or CMRGlu (Fig. S1).

ROT subjects exhibited substantial variability in their mean direction error (MDE) in response to imposed rotation. Critically, subjects' mean MDEs correlated strongly with changes in AG in BA44 (Fig. 8*C*). ROT subjects with larger MDEs showed larger increases in AG. In this analysis, CTRL subjects had lower MDEs and a reduction in AG. Overall, both AG (Fig. 8*C*) and resting-state functional connectivity (Fig. 5) were significantly related to MDEs (i.e., higher MDEs were associated with increased
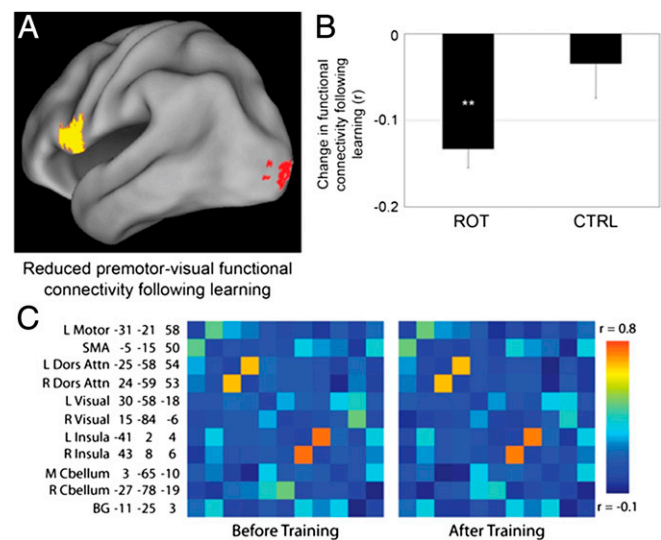

Fig. 4. Changes in premotor functional connectivity after task performance. (*A*) A whole-brain voxel-wise paired *t* test was performed to identify regions whose functional connectivity to left premotor cortex (yellow) was altered after task performance. A region in left V1 (red) shows a reduction in functional connectivity. (*B*) The premotor-V1 fcMRI change was specific to the ROT group. Correlation was reduced in the ROT group (**$P < 0.01$). Error bars represent SEM. (*C*) Correlations between eleven other task-recruited regions were calculated before and after task performance. The color of each square indicates the pairwise *r* value between the indicated regions. Very little difference is seen; no changes were statistically significant. The image shows pooled values including both ROT and CTRL groups; individual groups also did not show any significant changes.
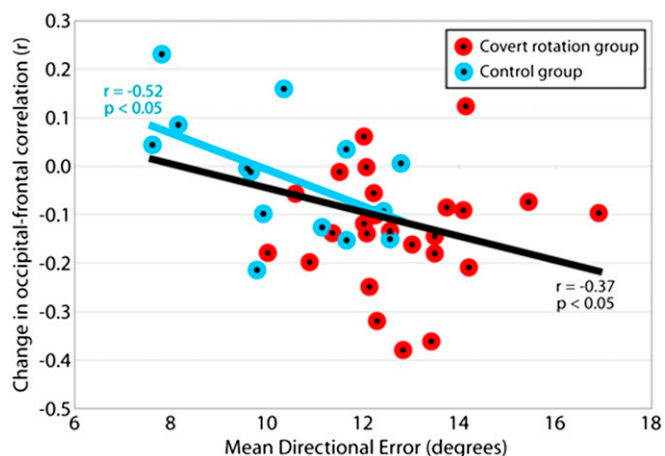
Fig. 5. Premotor-V1 functional connectivity changes depend on subject error rates. The scatter plot shows each subject's mean directional error against that subject's posttask minus pretask change in premotor-V1 functional connectivity. The relationship across all subjects is significantly negative (black bar), as is the relationship in the CTRL group alone (blue bar).

AG and decreased functional connectivity whereas lower MDEs were associated with decreased AG and increased functional connectivity).

Discussion

Overview. Our findings have led us to posit that the motor adaptation task we used induced Hebbian-like changes within the synaptic architecture of BA44 after task performance [long-term depression (LTD) in the ROT subjects and long-term potentiation (LTP) in the CTRL subjects]. Given our constellation of findings, we posit that the increase in aerobic glycolysis in the ROT group may well reflect, in part, synaptic pruning associated with LTD involving the action of activated microglia. The following discussion presents the evidence that led us to this view. We begin with a discussion of unique features of BA44 as revealed by fMRI and close with PET metabolic features of BA44.

Functional Magnetic Resonance Imaging. Despite being only one among many areas involved in task performance (Fig. 2) and only one of many areas sensitive to error-related task performance (Fig. 7), BA44 alone exhibited changes in resting-state functional connectivity and metabolism after task performance. BA44 is located immediately anterior to the ventralmost aspects of the motor homunculus. It is frequently classified as part of Broca's area, which is most closely associated with language generation (50–52) and the brain's language networks (53). However, this region is not exclusively recruited by language tasks. A wide range of fMRI experiments report recruitment of BA44 during a variety of difficult motor tasks (for review, see refs. 52 and 54). Fadiga et al. (54) suggest that BA44's role in language generation, which depends heavily on the precise coordination of lip, tongue, and diaphragm movements, is evolutionarily rooted in its role in performing complex motor tasks. Thus, it is not surprising that BA44 might show extensive involvement in the brain's adaptation to the visual–motor adaptation task. That an area of cerebral cortex should be involved early in the learning process is consistent with recent work by Bero et al. (55).

In the present experiment, left BA44 was recruited in both the ROT and CTRL groups (all right-handed) early in the training period. The CTRL group ultimately performed hundreds of out-and-back movements under consistent visual–motor feedback; in these subjects, fMRI responses in BA44 markedly attenuated by the end of training. In contrast, the ROT group was subjected to progressively incremented stylus-screen rotational mismatch. In these subjects, fMRI responses in BA44 were maintained throughout the training period.

Notably, BA44 behaves similarly when subjects perform lexical tasks in which the response is not automatic. During a "verb-generation" task in which subjects were presented with a common English noun and asked to generate an appropriate verb, left BA44 was strongly recruited when subjects first began the task. After extensive practice with the same list of nouns, recruitment of BA44 returned to baseline (56). Introduction of a novel list of words again recruited BA44. This result suggests that BA44 may be uniquely involved in high-level adaptive processing in response to performance of difficult novel tasks.

Performance of our out-and-back motor adaptation task relied heavily on communication between visual and motor systems. When this communication fails to produce accurate trajectories on the screen, whether because of experimenter-induced error or natural error as in our CTRL group, visual–motor communication is altered. Behavioral feedback in this case seems to occur nonconsciously to shape interregional relationships. Perhaps the most attractive explanation for the reduction in the strength of correlated spontaneous activity between BA44 and V1 in the ROT group is that it represents a weakening of synaptic transmission between BA 44 and V1 in the face of antecedent, task-evoked, presynaptic activity from V1 that failed to consistently correlate with postsynaptic activity in BA44. In other words, as the input from V1 continually failed to provide a correct, adaptive motor response, the brain reduced information transfer from that region. Theories of synaptic plasticity (57) as well as direct neurophysiological observations (58, 59) are consistent with our view.

It is important to note that CTRL subjects with the lowest error rates actually exhibited an increase in resting-state function connectivity, suggesting that change in resting-state functional connectivity may reflect Hebbian-like processes [i.e., long-term potentiation (LTP) and long-term depression (LTD); for reviews, see refs. 60–62] in which the outcome reflects a change in the balance between strengthening (LTP) and weakening (LTD) of synaptic relationships (63).

Our metabolic data, discussed below, indicated that the task-induced synaptic remodeling was confined to BA44. Contemporaneous with this remodeling, the task-evoked BOLD signal in BA44 remained elevated throughout the task in the ROT group. Previous work (56) has shown that activity in BA44 increases in response to novel or challenging stimuli, consistent with our observations. It is likely that visual cortex is just one of many brain regions providing input to BA44, in addition to the extensive local, internal connections found throughout the cortex. We believe a reduction of one of these inputs was not sufficient to noticeably change the measured BOLD signal in the region. More speculatively,
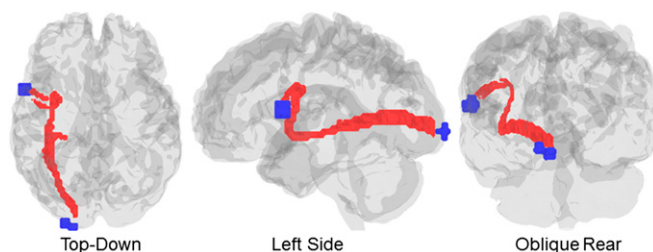

Fig. 6. White-matter tracts connecting V1 and BA44. Tract-tracing analysis was performed using DTI on a separate group of 30 healthy young adults. The resulting consensus tract (red) between the two regions (blue) is shown in dorsal, lateral, and posterior-oblique views.
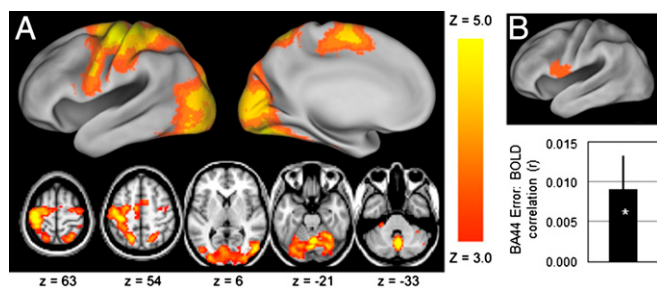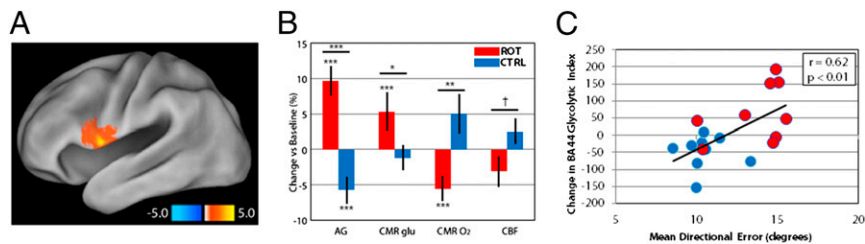
Fig. 7. Error-related activity changes during task performance. Mean error during each fMRI frame was entered as a term in the GLM to identify regions whose activity varied as a function of trajectory errors. (*A*) Motor-, vision-, and attention-related regions showed increases in activity after errors; these areas are very similar to those regions activated by simple task performance (Fig. 2). (*B*) A hypothesis-driven test in BA44 shows a significant relationship between error and BA44 activity (*$P < 0.05$).

it is possible that the ongoing activity seen in BA44 was itself a cause of the remodeling—that some aspects of this activity derived from neural signaling that guided synaptic changes.

Extensive work has investigated the significance of correlated fluctuations in spontaneous BOLD activity. One hypothesis argues that functional connectivity results from a lifetime history of coactivation of different brain regions (64). In the adult brain, the organization of spontaneous correlated activity broadly mirrors the topography of task-evoked responses (65–68). This conjunction suggests that Hebbian mechanisms arising in the context of spontaneous activity may dynamically shape relationships within and among functional networks, a hypothesis that receives support from direct neurophysiological observations (for example, see ref. 59). We review, briefly, evidence in support of this hypothesis from fMRI BOLD imaging studies of resting-state spontaneous activity.

Studies of functional connectivity after motor training or other forms of learning provide evidence for the adaptive nature of resting-state BOLD functional connectivity. For example, Stevens et al. (69) reported stronger coupling between the inferior frontal gyrus and face-preferential areas of the visual cortex after a face-recognition task, as well as stronger coupling between the inferior frontal gyrus and scene-specific visual areas after a scene-recognition task. Ma et al. (70), using independent component analysis after extended motor-sequence learning, showed increased strength in three motor-related components, which tracked behavioral improvement. A recent study by Mackey et al. (71) reported strengthened correlations between frontal and parietal attention and control regions in subjects who completed a lengthy preparation course for a law-school entrance examination. These studies reflect processes focusing on the strengthening of extant skills or the acquisition of an entirely new skill.

Other work reveals more complex task-induced changes in resting-state functional connectivity. Lewis et al. (72) trained subjects on a perceptual discrimination task. Task performance recruited a variety of regions, including early and late visual cortex and the frontal eye fields (FEFs), while reducing activity in the default-mode network (DMN). Functional connectivity was shown to decrease between early visual cortex and FEF, while increasing between higher order visual cortex and the DMN. Using a motor adaptation task, Vahdat et al. (73) reported a mixture of strengthened and weakened correlations between several motor-related regions after motor adaptation task training. Finally, Harmelech et al. (64) demonstrated that a single, 30-min episode of cortical activation induced a lasting restructuring of resting-state functional connectivity (both increases and decreases) according to a Hebbian-like rule.

Together with our own data, the above findings suggest that task-induced changes in functional connectivity observed with resting-state BOLD fMRI may represent alterations in information transfer between the regions. If so, this observation would extend the list of processes implicated in the development and ongoing maintenance of functional connectivity. Importantly, this observation would suggest that changes in resting-state functional connectivity may be an informative biomarker of synaptic plasticity. Our PET metabolism results provide supportive data for this hypothesis.

Metabolism. As described in the Introduction, several lines of evidence indicate that AG likely plays an important role in brain development and plasticity. This role is particularly dramatic in the developing human brain (20). Even in the adult human brain, regions high in AG exhibit gene expression typical of infancy [transcriptional neotony (20)]. Neotony is consistent with lifelong processes of synaptic proliferation and elimination (63, 74).

Our results are consistent with a link between plasticity and AG. The observed increases in AG after motor adaptation may reflect, in large part, the creation, elimination, and restructuring of synaptic connections. As described in the Introduction, the shunting of glucose away from oxidative phosphorylation provides molecular building blocks needed for synaptic plasticity. Surprisingly however, the increase in AG observed here in BA44 is not driven only by increased glucose consumption, but also by reduced oxygen consumption. Oxygen consumption is a direct measure of brain energy consumption (37), and its reduction, combined with the localized reduction in resting-state functional connectivity between BA44 and V1, is indicative of decreased synaptic activity in BA44 (75–77). The changes in glucose, oxygen, and functional connectivity suggest that both LTP and LTD may have occurred, with the net effect being an overall decrease in the number of synapses (78, 79).

These findings also constrain the link between neural activity and AG by showing that task-evoked AG (26, 34–36, 80) does not automatically lead to increased AG after task performance. Large areas in primary motor and visual cortex, for example (Fig. 2),

Fig. 8. BA44 exhibits increased aerobic glycolysis after motor adaptation. (*A*) Whole-brain PET analyses identified a region in left BA44 where aerobic glycolysis (AG) was increased in the ROT group but not the CTRL group. (*B*) Post hoc regional analyses indicate that AG is increased 10% relative to baseline in the ROT group. The change in glycolysis is driven by both an increase in glucose utilization ($CMRGlu$) as well as a reduction in oxygen consumption ($CMRO_2$). Cerebral blood flow (CBF) shows a nonsignificant trend toward reduction. Error bars represent SEM (***$P < 0.001$; **$P < 0.01$; *$P < 0.05$; and †$P = 0.056$). (*C*) Subjectwise correlation between change in BA44 glycolytic index [a measure of tissue AG (21)] and motor adaptation rates. Subjects who adapted faster showed larger increases in glycolysis ($r = 0.80$, $P < 0.01$ two-tailed). Given recent concerns about the robustness of correlations computed on small sample sizes (119), this r value should be interpreted cautiously.

Shannon et al.

were activated during the task in an error-dependent manner (Fig. 7), but did not show subsequent increases in AG. It was only in BA44 that a sustained increase in AG was observed (Fig. S2). Note that our calculation of AG is based on local-to-global ratios, unlike Madsen et al. (26), who calculated whole-brain values. Thus, we cannot exclude a whole-brain increase in AG. However, we can exclude a simple task-activity/AG correspondence. This regional specificity indicates that extended periods of increased AG come about as a consequence of learning-induced changes in the functional architecture of the brain, rather than changes in global energy demands.

Notably, we observed no significant changes to metabolism in the cerebellum. The cerebellum is closely associated with motor performance and motor learning and is active during a variety of motor learning tasks (for a review, see ref. 81). Portions of the cerebellum exhibited increased fMRI BOLD signal during our task (Fig. S3), but, in contrast to BA44, these increases did not persist 2 h later during the PET scans. Such dissociations between immediate and hours-later responses to learning experiences have been documented in other learning paradigms (e.g., ref. 55). One possibility is that synapses within the cerebellum itself were not substantially remodeled. Instead, the cerebellum may have contributed to motor adaptation by altering activity rather than synaptic structure, or by influencing other brain regions. Alternatively, changes to cerebellar metabolism may have been too small in magnitude or too localized for our techniques to detect. Unlike the cerebral cortex, practically no AG occurs in the cerebellum at rest (21). The cerebellum also expresses relatively few neotenous genes (63).

The cellular processes involved in synaptic elimination include localized, mitochondrial-mediated apoptosis in dendritic spines (82–84) that trigger immune functions mediated by the complement system (85, 86), which, in turn, initiate the removal of synaptic detritus by microglia (87–91) and possibly even astrocytes (92).

Microglia have traditionally been thought of as the immune cells of the brain, but a body of recent research suggests that these cells may also play important roles in nonpathological brain function, specifically the pruning and alteration of synapses (90). Animal live-imaging studies have demonstrated that microglia interact dynamically with synapses undergoing developmental pruning (93, 94). Dendritic spines that were touched by microglia tended to shrink or disappear. Fluorescent tagging of synaptic components showed that these components were often phagocytosed by microglia during plasticity (87). We suspect that these events are occurring in BA44 after human motor adaptation.

We call attention to activated microglia as potential contributors to the localized increase in AG in BA44 in ROT subjects because of the changes in metabolism likely associated with their activation. As with immune cells elsewhere in the body (17, 18, 95), microglia can exist in a surveillant state as well as an activated state (19, 95). The activated state of microglia (19) as well as other immune cells (95) is characterized by a metabolic shift from oxidative phosphorylation to a greater reliance on AG enabling proliferation as well as enhanced functionality. This shift in metabolism toward a greater emphasis on AG might well be occurring with support from astrocytes (96) that are well known for their contributions to brain AG (for a recent comprehensive review, see ref. 97).

Further support for our hypothesis comes from our CTRL group. They too exhibited learning-related changes after performance of the unmanipulated version of the motor task. In BA44, oxygen consumption increased, AG was reduced, and, among those subjects with very low error rates, functional connectivity with V1 increased. The magnitude of the latter two findings correlated with subjects' behavioral performance. From a Hebbian perspective, these changes would be consistent with LTP, not LTD. In this regard, it is of interest that LTP inhibits LTD in rat hippocampal slices for at least an hour (98), an effect

mediated by the inhibition of GSK3β, a multifunctional enzyme and signaling protein (99) first described as a facilitator of glycogenolysis (100).

Proliferation and elimination of synapses exist in a dynamic balance in the adult brain as reflected at the process level in LTP and LTD (101) and at the genetic level in genes associated with proliferation and elimination (63). Homeostasis is critical. We see evidence of homeostasis in our results when comparing our CTRL group with our ROT group. The fact that AG is actually down-regulated in the CTRL group was initially puzzling but might well be viewed as a shift in the balance between LTP and LTD in which AG continuously plays a role in both biosynthesis and synaptic pruning, processes mechanistically mediated by the specific cell type by which the process is mediated (i.e., neurons and various glial cell types).

So, how might it be determined experimentally whether activated microglia are, in fact, playing a role in our experiments? Fortuitously, several PET tracers exist that are specific markers for activated microglia. Active microglia abundantly express the peripheral benzodiazepine receptor (PBR) (102), and ^{11}C-tagged PET tracers PK11195 and PBR28 bind to PBR. Increases in tracer binding have been observed in humans in a wide variety of brain disease states involving inflammation, an important factor in activating microglia and other cells of the immune system, including Alzheimer's, HIV, multiple sclerosis, and stroke (102, 103). PBR imaging seems to be a robustly successful method for observing microglial activity during pathology-related inflammation. A logical test of our hypothesis would be to use PK11195 or PBR28 to detect the presence of activated microglia in BA44 after motor adaptation learning, an equally important nonpathological role for microglia.

Conclusion

In response to failed predictions in a visual–motor transformation task, the brain adaptively and selectively reorganizes itself. We see evidence of synaptic plasticity through complementary changes in AG and oxygen consumption, as well as the functional consequences of this plasticity in altered task-evoked and resting-state activity. We believe these changes are an example of the brain managing interregional information transfer to optimize predictive accuracy. These measures of metabolism and ongoing functional organization, those changes elicited by both experimental demands as well as ongoing activity, likely serve as measurable in vivo biomarkers of neural plasticity. Performing such work in humans speaks to the challenge of understanding neural plasticity at a more holistic level. As Malenka and Bear (60) noted, "... it remains a challenging task to demonstrate that an in vivo experience generates LTP or LTD at some specific set of synapses and that this synaptic modification plays an important function role."

Methods

Subjects. Forty-six healthy, right-handed neurologically normal participants were recruited from the Washington University community (24 women; mean age 24.4 y). Data from the PET experiments come from a subgroup of 18 subjects. These subjects were scanned using PET before and after performing the motor adaptation task. We also obtained resting-state fMRI scans on these subjects before and after task performance. They were not scanned during task performance.

The remaining 28 subjects did not participate in PET scans. We scanned these subjects using fMRI during task performance and also obtained resting-state fMRI scans before and after task. All experiments were approved by the Human Research Protection Office and Radioactive Drug Research Committee at Washington University in St. Louis. Informed consent was obtained from all participants.

Motor Learning Task. The motor learning task was an out-and-back reaching movement task (eTT) that was performed using an MRI-compatible stylus and digitizing tablet (Mag Design and Engineering). This task has been used extensively during functional imaging to study motor adaptation (45, 104, 105).

www.manaraa.com

Subjects viewed a computer monitor that displayed a central fixation point and eight surrounding circles. An on-screen cursor was controlled by the hand-held stylus. Each trial began with one of the eight surrounding circles changing from white to black. Subjects were instructed to move the cursor from the central fixation point to the cued circle and back to the center as quickly and accurately as possible. Trials occurred in rapid succession every 1,080 ms, in synchrony with the fMRI acquisitions (two trials per fMRI frame; see *fMRI Image Acquisition* below). Each of the surrounding circles was cued in a pseudorandom order. Stimulus blocks comprised 264 out-and-back movements.

Covert Motor Learning. Subjects were randomized into two groups: a covert rotation learning group (ROT) and a control group (CTRL). While ROT subjects performed the task, we gradually and covertly imposed a rotation on the mapping between the stylus and the display screen. Rotation was imposed in 15° steps over the course of the session up to a maximum of 60°, as shown in Fig. 2. Subjects generally were unaware of this rotation (45). CTRL subjects performed the task with no rotation.

Accuracy on each trial was assessed by identifying the moment at which the stylus was moving at peak speed and calculating the instantaneous directional error (the angular difference between the stylus trajectory and a straight line directly to the target). Trials in which the cursor did not originate or return to the central circle, or in which peak-speed directional error was greater than 60°, were not interpretable and were discarded from further analyses. For each subject, an error rate was calculated by averaging the absolute value of the directional error across all trials. For the ROT subjects, an adaptation rate was calculated by using linear regression to estimate the rate at which directional error was reduced over the first 50 trials.

PET Image Acquisition. We obtained measures of CMRGlu, $CMRO_2$, and CBF before and after task performance. The pretask PET session was typically conducted between 08:30 and 10:30. The subjects were then transported to another laboratory where the covert motor learning task was administered between 1130 and 1230. The posttask PET session commenced at ∼1400 and was completed within 2 h.

Acquisition and processing techniques were similar to techniques described in our previous work (21, 106). Before each PET session, an antecubital i.v. catheter was placed in the arm for tracer injection and blood sampling for glucose levels. Each PET session lasted approximately 3 h and consisted of seven PET scans and two transmission scans. The first transmission scan was acquired before any PET scans. Before the first PET scan, subjects were asked to inhale 40–75 mCi of radioactive carbon monoxide. Before the second PET scan, subjects were asked to inhale 40–75 mCi of radioactive oxygen. Before the third PET scan, subjects were injected with 25–50 mCi of radioactive water. The fourth to sixth PET scans were repetitions of the first to third scans. A second transmission scan was then acquired. For the seventh PET scan, a measurement of cerebral metabolic rate of glucose (CMRGlu) was initiated with an ∼20-s bolus i.v. injection of 5 mCi of [^{18}F]fluorodeoxyglucose (FDG), immediately followed by a concomitant 60-min dynamic scan. Dynamic acquisition of PET emission data continued for 60 min with 25 5-s frames, 10 1-min frames, and nine 5-min frames. Before the injection of FDG, a blood sample was withdrawn for measurement of glucose. A second blood sample was withdrawn 30 min from the start of the FDG scan. All scans were obtained in the resting state; subjects were asked to lie quietly with their eyes closed. Investigators spoke to subjects briefly between each scan and at 15-min intervals during the FDG scan to ensure the subjects had not fallen asleep.

PET Analysis. Measures of brain metabolism were calculated from PET data using well-characterized techniques (21). We did not compute absolute levels of metabolism, but rather analyzed regional activity by calculating local-to-global ratios. In each subject, voxel-wise CBF, $CMRO_2$ and CMRGlu values were scaled to a whole-brain mean of one. CBF was measured with a 40-s emission image (derived from a 120-s dynamic scan) after rapid injection of [^{15}O]-water in saline (107, 108). CBV was measured with a 5-min emission scan beginning 2 min after brief inhalation of [^{15}O]-carbon monoxide in room air (108, 109). $CMRO_2$ was measured with a 40-s emission scan (derived from a 120-s dynamic scan) after brief inhalation of [^{15}O]-oxygen in room air (108, 110). FDG uptake and trapping were used to image CMRGlu (34). Parametric images of net FDG trapping were created by application of the Patlak graphical method (111, 112). Individual subject data were registered to Talairach atlas space using high-resolution T1- and T2-weighted structural MRI scans.

fMRI Image Acquisition. MRI studies were performed on a Siemens 3T Allegra. Imaging sessions began with acquisition of a three-orthogonal-slice scout,

followed by a coarse 3D T1-weighted magnetization-prepared rapid gradient echo (MPRAGE) structural image [echo time (TE) 3.93 ms, repetition time (TR) 722 ms, inversion time (TI) 380 ms, flip angle 8°, 128 × 28 acquisition matrix, 80 slices, 2 × 2 × 2-mm cubic voxels), used to position the field of view for subsequent acquisitions. High-resolution structural images were acquired using a 3D sagittal T1-weighted MPRAGE acquisition optimized for high contrast-to-noise ratio and resolution (TE 3.93 ms, TR 1,900 ms, 256 × 256 acquisition matrix, 160 slices, 1 × 1 × 1-mm cubic voxels). High-resolution 2D multislice oblique axial spin-density/T2-weighted turbo spin echo (TSE) structural images (TE 98 ms, TR 2,100 ms) were also acquired and subsequently used during atlas transformation of the fMRI data. Functional images were collected using an echo-planar sequence sensitive to BOLD contrast (TE 25 ms, TR 2,160 ms, 256 × 256 acquisition matrix, 39 slices, 4 × 4 × 4-mm cubic voxels), acquired parallel to the anterior–posterior commissure plane.

Task fMRI Analysis. fMRI data were preprocessed and transformed to Talairach atlas space using previously described techniques (113). Task-related activity was estimated using a general linear model (GLM) to estimate hemodynamic responses to task blocks. Pretraining, training, and posttraining blocks were each modeled separately. Two ANOVA analyses were performed. First, the ROT and CTRL groups were pooled, and a main effect of time analysis was performed to identify voxels in which the task structure significantly accounted for signal variance (i.e., task-evoked responses). A second ANOVA contrasted pre- vs. posttraining in the ROT vs. CTRL groups (time × pre/post × ROT/CTRL interaction). F-statistic maps were converted to equiprobable Z-scores and corrected for multiple comparisons by identifying contiguous clusters of voxels satisfying predefined threshold-extent criteria (Z > 3.0, cluster size > 17, P < 0.01).

Resting-State fMRI Analysis. Eyes-closed resting-state scans were acquired in all subjects before and after task performance. Two 194-frame (7-min) runs were obtained in each condition, yielding a total of 28 min of resting-state data. Preprocessing was performed as described previously (114). Functional connectivity-specific preprocessing included low-pass temporal filtering (one-half frequency = 0.1 Hz), spatial blurring (Gaussian kernel, 6-mm full-width half-max in each direction), and removal by regression of nuisance signals extracted from bilateral regions in white matter (cingulum; centered at ±32, −20, 30) and the lateral ventricles (±6, −10, 20), plus rigid-body parameters derived from retrospective head movement correction. The mean signal averaged over the whole brain was also included as a regressor of no interest [global signal regression (GSR)]. Thus, each correlation map was approximately zero-centered (114). Frames contaminated by excessive head motion were identified and excluded from functional connectivity analysis (>3 SD frame-to-frame whole-brain signal change) (115). No subjects were entirely excluded due to excessive movement. Pearson correlations were Fisher z-transformed [generating z(r) values] before subsequent analyses.

Resting-state functional connectivity measurements with fMRI are exquisitely sensitive to head motion (115, 116). We note that head motion was slightly greater during later scans, as is typical in relatively long fMRI sessions. Although considerable care was taken to minimize the impact of head motion on our functional connectivity measurements (116), residual motion-induced artifacts may have been present. However, head motion was comparable in the CTRL and ROT groups. Therefore, this factor is unlikely to account for the differential effects of imposed rotation.

Differences between pre- and posttraining resting-state functional connectivity were assessed in two ways. First, an exploratory analysis was performed on the ROT group data, to probe whether training-related alterations in AG were also reflected in resting-state BOLD time series. The region of BA44 showing increased AG was used as a seed. Correlation maps were computed using standard techniques, and voxel-wise paired *t* tests were applied to the pre- vs. posttraining contrast. Multiple comparison correction was performed through value- and extent-thresholding, determined by Monte Carlo permutation simulation (Z > 4.0, cluster size > 10) (117). In brief, simulations were run in which some randomly selected subjects' pre- and posttraining correlation maps were switched before the *t* test was performed. In these simulated results, we tested whether any clusters existed that exceeded the specified Z-score and size thresholds. This simulation was repeated 10,000 times, and the fraction of simulations containing above-threshold clusters corresponded to the P value of the specified thresholds.

This exploratory analysis identified a region in left V1 whose functional connectivity with BA44 was reduced after task performance in the ROT group. In a post hoc analysis, we calculated BA44:V1 correlation values for each subject in both the ROT and CTRL groups, and determined (by paired *t* test) whether this effect was also present in the CTRL group, as well as whether the effect differed between groups (mixed-effects interaction).

Shannon et al.

Second, we assessed the effect of task performance on functional connectivity between regions recruited by the task. These regions were defined by identifying peak values in the main effect of time ANOVA described above. Peak loci closer than 20-mm Euclidean distance were consolidated into a single locus at the cluster center of mass. Regions were created as 6-mm-radius spheres, drawn about the center of these peaks, excluding voxels with Z values below 6.0. This procedure identified a set of 11 regions, comprising visual, motor, and attention-related areas (Fig. 5C). An 11×11 cross-correlation matrix was calculated for this set of regions, separately for each individual's pre- and posttraining resting scans. Training effects were assessed by computing a paired t test between each set of regions. Bonferroni multiple-comparison correction was applied (final threshold = $P < 0.0009$).

Error-Related Changes in Functional Connectivity. Subjects varied considerably in their task accuracy. We tested whether this accuracy might be related to observed training-induced changes in BA44:V1 functional connectivity. We calculated each subject's error rate as the mean absolute value of angular error (Motor Learning Task) during the training runs. We tested whether error rates were correlated with each subject's change in BA44:V1 functional connectivity (pretraining r value minus posttraining r value). These correlations were tested separately for the ROT and CTRL groups, as well as a pool containing all subjects. Statistical significance was assessed using a standard r-to-P transformation.

Error-Related Activity. We examined fMRI activity during task performance to test for reliable activity changes related to movement accuracy on a trial-by-trial basis. To this end, we included an additional error-related regressor in the GLM. This regressor consisted of the mean absolute directional error for each frame, shifted by two frames to account for hemodynamic delay. The GLM was recalculated with this component, and error-activity maps were

generated for each subject. These maps, pooled across ROT and CTRL groups, were entered into a random-effects model to calculate a group Z-statistic map. This map was value- and extent-thresholded to a corrected P value of 0.05 ($Z > 3.0$, cluster size > 200).

Diffusion Tensor Imaging Tracking. DTI scans from a normal control group obtained for a different study (44) were reanalyzed ($n = 30$). The DTI data were obtained on a Trio 3T scanner (Siemens) with 63 measurement directions, 2-mm cubic voxels, and b values of 1,000 s/mm^2. DTI and tracking computations were performed using FSL diffusion toolbox (47). Each individual's DTI dataset was motion-corrected using a 9-parameter affine registration (FLIRT), aligned, and averaged, and then a brain mask (BET) was computed. Diffusion parameters were computed, and tracking was performed using FDT (118).

To map out the track of interest, both the start point region of interest (ROI) (occipital lobe, visual cortex) and end point ROI (BA44) were mapped into each individual's native space, and probabilistic tractography was performed separately for each subject. Each connectivity map was then thresholded to remove extraneous pathways and then converted into a binary mask representing the tract volume for that subject. These tract volumes were then transformed back to atlas space and averaged across all subjects to create an average anatomic atlas representation of the tract of interest presented in Fig. 6.

1. Siesjo BK (1978) *Brain Energy Metabolism* (John Wiley, New York).
2. Raichle ME, Posner JB, Plum F (1970) Cerebral blood flow during and after hyperventilation. *Arch Neurol* 23(5):394–403.
3. Boyle PJ, et al. (1994) Diminished brain glucose metabolism is a significant determinant for falling rates of systemic glucose utilization during sleep in normal humans. *J Clin Invest* 93(2):529–535.
4. Powers WJ, et al. (2007) Selective defect of in vivo glycolysis in early Huntington's disease striatum. *Proc Natl Acad Sci USA* 104(8):2945–2949.
5. Mintun MA, et al. (2001) Blood flow and oxygen delivery to human brain during functional activity: Theoretical modeling and experimental data. *Proc Natl Acad Sci USA* 98(12):6859–6864.
6. Vander Heiden MG, Cantley LC, Thompson CB (2009) Understanding the Warburg effect: The metabolic requirements of cell proliferation. *Science* 324(5930):1029–1033.
7. Locasale JW, Cantley LC (2011) Metabolic flux and the regulation of mammalian cell growth. *Cell Metab* 14(4):443–451.
8. Lunt SY, Vander Heiden MG (2011) Aerobic glycolysis: Meeting the metabolic requirements of cell proliferation. *Annu Rev Cell Dev Biol* 27:441–464.
9. Brand KA, Hermfisse U (1997) Aerobic glycolysis by proliferating cells: A protective strategy against reactive oxygen species. *FASEB J* 11(5):388–395.
10. Cerdán S, et al. (2006) The redox switch/redox coupling hypothesis. *Neurochem Int* 48(6-7):523–530.
11. Vaughn AE, Deshmukh M (2008) Glucose metabolism inhibits apoptosis in neurons and cancer cells by redox inactivation of cytochrome c. *Nat Cell Biol* 10(12):1477–1483.
12. Mercer RW, Dunham PB (1981) Membrane-bound ATP fuels the Na/K pump: Studies on membrane-bound glycolytic enzymes on inside-out vesicles from human red cell membranes. *J Gen Physiol* 78(5):547–568.
13. Okamoto K, Wang W, Rounds J, Chambers EA, Jacobs DO (2001) ATP from glycolysis is required for normal sodium homeostasis in resting fast-twitch rodent skeletal muscle. *Am J Physiol Endocrinol Metab* 281(3):E479–E488.
14. Campbell JD, Paul RJ (1992) The nature of fuel provision for the Na+,K(+)-ATPase in porcine vascular smooth muscle. *J Physiol* 447:67–82.
15. Nichols CG (2006) KATP channels as molecular sensors of cellular metabolism. *Nature* 440(7083):470–476.
16. Macauley SL, et al. (2015) Hyperglycemia modulates extracellular amyloid-β concentrations and neuronal activity in vivo. *J Clin Invest* 125(6):2463–2467.
17. Chang CH, et al. (2013) Posttranscriptional control of T cell effector function by aerobic glycolysis. *Cell* 153(6):1239–1251.
18. Pearce EL, Poffenberger MC, Chang CH, Jones RG (2013) Fueling immunity: Insights into metabolism and lymphocyte function. *Science* 342(6155):1242454.
19. Orihuela R, McPherson CA, Harry GJ (2016) Microglial M1/M2 polarization and metabolic states. *Br J Pharmacol* 173(4):649–665.
20. Goyal MS, Hawrylycz M, Miller JA, Snyder AZ, Raichle ME (2014) Aerobic glycolysis in the human brain is associated with development and neotenous gene expression. *Cell Metab* 19(1):49–57.
21. Vaishnavi SN, et al. (2010) Regional aerobic glycolysis in the human brain. *Proc Natl Acad Sci USA* 107(41):17757–17762.
22. Raichle ME (2015) The restless brain: How intrinsic activity organizes brain function. *Philos Trans R Soc Lond B Biol Sci* 370(1668):1–11.
23. Suzuki A, et al. (2011) Astrocyte-neuron lactate transport is required for long-term memory formation. *Cell* 144(5):810–823.
24. Newman LA, Korol DL, Gold PE (2011) Lactate produced by glycogenolysis in astrocytes regulates memory processing. *PLoS One* 6(12):e28427.
25. Yang J, et al. (2014) Lactate promotes plasticity gene expression by potentiating NMDA signaling in neurons. *Proc Natl Acad Sci USA* 111(33):12228–12233.
26. Madsen PL, et al. (1995) Persistent resetting of the cerebral oxygen/glucose uptake ratio by brain activation: Evidence obtained with the Kety-Schmidt technique. *J Cereb Blood Flow Metab* 15(3):485–491.
27. Kety SS, Schmidt CF (1948) The nitrous oxide method for the quantitative determination of cerebral blood flow in man: Theory, procedure and normal values. *J Clin Invest* 27(4):476–483.
28. Berg EA (1948) A simple objective technique for measuring flexibility in thinking. *J Gen Psychol* 39:15–22.
29. Grant DA, Berg EA (1948) A behavioral analysis of degree of reinforcement and ease of shifting to new responses in a Weigl-type card-sorting problem. *J Exp Psychol* 38(4):404–411.
30. Milner B (1963) Effects of different brain lesions on card sorting. *Arch Neurol* 9:90–100.
31. Basso MR, Lowery N, Ghormley C, Bornstein RA (2001) Practice effects on the Wisconsin Card Sorting Test-64 Card version across 12 months. *Clin Neuropsychol* 15(4):471–478.
32. Bird CM, Papadopoulou K, Ricciardelli P, Rossor MN, Cipolotti L (2004) Monitoring cognitive changes: Psychometric properties of six cognitive tests. *Br J Clin Psychol* 43(Pt 2):197–210.
33. Paolo AM, Axelrod BN, Troster AI (1996) Test-retest stability of the Wisconsin Card Sorting Test. *Assessment* 3(2):137–143.
34. Fox PT, Raichle ME, Mintun MA, Dence C (1988) Nonoxidative glucose consumption during focal physiologic neural activity. *Science* 241(4864):462–464.
35. Bero AW, et al. (2011) Neuronal activity regulates the regional vulnerability to amyloid-β deposition. *Nat Neurosci* 14(6):750–756.
36. Blomqvist G, et al. (1994) Regional cerebral oxidative and total glucose consumption during rest and activation studied with positron emission tomography. *Acta Physiol Scand* 151(1):29–43.
37. Raichle ME, Mintun MA (2006) Brain work and brain imaging. *Annu Rev Neurosci* 29:449–476.
38. Pellerin L, Magistretti PJ (2012) Sweet sixteen for ANLS. *J Cereb Blood Flow Metab* 32(7):1152–1166.
39. Kety SS, Schmidt CF (1946) The effects of active and passive hyperventilation on cerebral blood flow, cerebral oxygen consumption, cardiac output, and blood pressure of normal young men. *J Clin Invest* 25(1):107–119.
40. von Helmholtz H (1924) [*Helmholtz's Treatise on Physiological Optics*] (George Manta, Menasha, WI); trans Southall, 3rd Ed.
41. Newport R, Schenk T (2012) Prisms and neglect: What have we learned? *Neuropsychologia* 50(6):1080–1091.
42. Neves G, Cooke SF, Bliss TV (2008) Synaptic plasticity, memory and the hippocampus: A neural network approach to causality. *Nat Rev Neurosci* 9(1):65–75.
43. Whitlock JR, Heynen AJ, Shuler MG, Bear MF (2006) Learning induces long-term potentiation in the hippocampus. *Science* 313(5790):1093–1097.

www.manaraa.com

44. Siegel JS, Snyder AZ, Ramsey L, Shulman GL, Corbetta M (2015) The effects of hemodynamic lag on functional connectivity and behavior after stroke. *J Cereb Blood Flow Metab*, in press.

45. Ghilardi M, et al. (2000) Patterns of regional brain activation associated with different forms of motor learning. *Brain Res* 871(1):127–145.

46. Redding GM, Wallace B (1993) Adaptive coordination and alignment of eye and hand. *J Mot Behav* 25(2):75–88.

47. Smith SM, et al. (2004) Advances in functional and structural MR image analysis and implementation as FSL. *Neuroimage* 23(Suppl 1):S208–S219.

48. McAvoy MP, Ollinger JM, Buckner RL (2001) Cluster size thresholds for assessment of significant activation in fMRI. *Neuroimage* 13(Suppl 6):198.

49. Forman SD, et al. (1995) Improved assessment of significant activation in functional magnetic resonance imaging (fMRI): Use of a cluster-size threshold. *Magn Reson Med* 33(5):636–647.

50. Price CJ (2012) A review and synthesis of the first 20 years of PET and fMRI studies of heard speech, spoken language and reading. *Neuroimage* 62(2):816–847.

51. Dronkers NF (1996) A new brain region for coordinating speech articulation. *Nature* 384(6605):159–161.

52. Jeon HA, Friederici AD (2015) Degree of automaticity and the prefrontal cortex. *Trends Cogn Sci* 19(5):244–250.

53. Hacker CD, et al. (2013) Resting state network estimation in individual subjects. *Neuroimage* 82:616–633.

54. Fadiga L, Craighero L, D'Ausilio A (2009) Broca's area in language, action, and music. *Ann N Y Acad Sci* 1169:448–458.

55. Bero AW, et al. (2014) Early remodeling of the neocortex upon episodic memory encoding. *Proc Natl Acad Sci USA* 111(32):11852–11857.

56. Raichle ME, et al. (1994) Practice-related changes in human brain functional anatomy during nonmotor learning. *Cereb Cortex* 4(1):8–26.

57. Bienenstock EL, Cooper LN, Munro PW (1982) Theory for the development of neuron selectivity: Orientation specificity and binocular interaction in visual cortex. *J Neurosci* 2(1):32–48.

58. Jacob V, Brasier DJ, Erchova I, Feldman D, Shulz DE (2007) Spike timing-dependent synaptic depression in the in vivo barrel cortex of the rat. *J Neurosci* 27(6):1271–1284.

59. Winnubst J, Cheyne JE, Niculescu D, Lohmann C (2015) Spontaneous activity drives local synaptic plasticity in vivo. *Neuron* 87(2):399–410.

60. Malenka RC, Bear MF (2004) LTP and LTD: An embarrassment of riches. *Neuron* 44(1):5–21.

61. Citri A, Malenka RC (2008) Synaptic plasticity: Multiple forms, functions, and mechanisms. *Neuropsychopharmacology* 33(1):18–41.

62. Südhof TC, Malenka RC (2008) Understanding synapses: Past, present, and future. *Neuron* 60(3):469–476.

63. Goyal MS, Raichle ME (2013) Gene expression-based modeling of human cortical synaptic density. *Proc Natl Acad Sci USA* 110(16):6571–6576.

64. Harmelech T, Preminger S, Wertman E, Malach R (2013) The day-after effect: Long term, Hebbian-like restructuring of resting-state fMRI patterns induced by a single epoch of cortical activation. *J Neurosci* 33(22):9488–9497.

65. Biswal B, Yetkin FZ, Haughton VM, Hyde JS (1995) Functional connectivity in the motor cortex of resting human brain using echo-planar MRI. *Magn Reson Med* 34(4):537–541.

66. Fox MD, et al. (2005) The human brain is intrinsically organized into dynamic, anticorrelated functional networks. *Proc Natl Acad Sci USA* 102(27):9673–9678.

67. Mennes M, et al. (2010) Inter-individual differences in resting-state functional connectivity predict task-induced BOLD activity. *Neuroimage* 50(4):1690–1701.

68. Mennes M, Kelly C, Colcombe S, Castellanos FX, Milham MP (2013) The extrinsic and intrinsic functional architectures of the human brain are not equivalent. *Cereb Cortex* 23(1):223–229.

69. Stevens WD, Buckner RL, Schacter DL (2010) Correlated low-frequency BOLD fluctuations in the resting human brain are modulated by recent experience in category-preferential visual regions. *Cereb Cortex* 20(8):1997–2006.

70. Ma L, et al. (2010) Changes in regional activity are accompanied with changes in inter-regional connectivity during 4 weeks motor learning. *Brain Res* 1318(9):64–76.

71. Mackey AP, Miller Singley AT, Bunge SA (2013) Intensive reasoning training alters patterns of brain connectivity at rest. *J Neurosci* 33(11):4796–4803.

72. Lewis CM, Baldassarre A, Committeri G, Romani GL, Corbetta M (2009) Learning sculpts the spontaneous activity of the resting human brain. *Proc Natl Acad Sci USA* 106(41):17558–17563.

73. Vahdat S, Darainy M, Milner TE, Ostry DJ (2011) Functionally specific changes in resting-state sensorimotor networks after motor learning. *J Neurosci* 31(47):16907–16915.

74. Marder E, Goaillard JM (2006) Variability, compensation and homeostasis in neuron and network function. *Nat Rev Neurosci* 7(7):563–574.

75. Schwartz WJ, et al. (1979) Metabolic mapping of functional activity in the hypothalamo-neurohypophysial system of the rat. *Science* 205(4407):723–725.

76. Kadekaro M, Crane AM, Sokoloff L (1985) Differential effects of electrical stimulation of sciatic nerve on metabolic activity in spinal cord and dorsal root ganglion in the rat. *Proc Natl Acad Sci USA* 82(17):6010–6013.

77. Kennedy C, et al. (1976) Metabolic mapping of the primary visual system of the monkey by means of the autoradiographic [14C]deoxyglucose technique. *Proc Natl Acad Sci USA* 73(11):4230–4234.

78. Holtmaat A, Svoboda K (2009) Experience-dependent structural synaptic plasticity in the mammalian brain. *Nat Rev Neurosci* 10(9):647–658.

79. Wiegert JS, Oertner TG (2013) Long-term depression triggers the selective elimination of weakly integrated synapses. *Proc Natl Acad Sci USA* 110(47):E4510–E4519.

80. Kasischke KA, Vishwasrao HD, Fisher PJ, Zipfel WR, Webb WW (2004) Neural activity triggers neuronal oxidative metabolism followed by astrocytic glycolysis. *Science* 305(5680):99–103.

81. Stoodley CJ (2012) The cerebellum and cognition: Evidence from functional imaging studies. *Cerebellum* 11(2):352–365.

82. Hyman BT, Yuan J (2012) Apoptotic and non-apoptotic roles of caspases in neuronal physiology and pathophysiology. *Nat Rev Neurosci* 13(6):395–406.

83. Li Z, Sheng M (2012) Caspases in synaptic plasticity. *Mol Brain* 5:15.

84. Li Z, et al. (2010) Caspase-3 activation via mitochondria is required for long-term depression and AMPA receptor internalization. *Cell* 141(5):859–871.

85. Stevens B, et al. (2007) The classical complement cascade mediates CNS synapse elimination. *Cell* 131(6):1164–1178.

86. Shatz CJ (2009) MHC class I: An unexpected role in neuronal plasticity. *Neuron* 64(1):40–45.

87. Schafer DP, et al. (2012) Microglia sculpt postnatal neural circuits in an activity and complement-dependent manner. *Neuron* 74(4):691–705.

88. Kettenmann H, Kirchhoff F, Verkhratsky A (2013) Microglia: New roles for the synaptic stripper. *Neuron* 77(1):10–18.

89. Williams DW, Kondo S, Krzyzanowska A, Hiromi Y, Truman JW (2006) Local caspase activity directs engulfment of dendrites during pruning. *Nat Neurosci* 9(10):1234–1236.

90. Schafer DP, Stevens B (2015) Microglia function in central nervous system development and plasticity. *Cold Spring Harb Perspect Biol* 7(10):a020545.

91. Gomez-Nicola D, Perry VH (2015) Microglial dynamics and role in the healthy and diseased brain: A paradigm of functional plasticity. *Neuroscientist* 21(2):169–184.

92. Chung WS, et al. (2013) Astrocytes mediate synapse elimination through MEGF10 and MERTK pathways. *Nature* 504(7480):394–400.

93. Tremblay ME, Lowery RL, Majewska AK (2010) Microglial interactions with synapses are modulated by visual experience. *PLoS Biol* 8(11):e1000527.

94. Wake H, Moorhouse AJ, Miyamoto A, Nabekura J (2013) Microglia: Actively surveying and shaping neuronal circuit structure and function. *Trends Neurosci* 36(4):209–217.

95. Pearce EL, Pearce EJ (2013) Metabolic pathways in immune cell activation and quiescence. *Immunity* 38(4):633–643.

96. Davalos D, et al. (2005) ATP mediates rapid microglial response to local brain injury in vivo. *Nat Neurosci* 8(6):752–758.

97. Bélanger M, Allaman I, Magistretti PJ (2011) Brain energy metabolism: Focus on astrocyte-neuron metabolic cooperation. *Cell Metab* 14(6):724–738.

98. Peineau S, et al. (2007) LTP inhibits LTD in the hippocampus via regulation of GSK3beta. *Neuron* 53(5):703–717.

99. Doble BW, Woodgett JR (2003) GSK-3: Tricks of the trade for a multi-tasking kinase. *J Cell Sci* 116(Pt 7):1175–1186.

100. Embi N, Rylatt DB, Cohen P (1980) Glycogen synthase kinase-3 from rabbit skeletal muscle: Separation from cyclic-AMP-dependent protein kinase and phosphorylase kinase. *Eur J Biochem* 107(2):519–527.

101. Turrigiano GG, Nelson SB (2004) Homeostatic plasticity in the developing nervous system. *Nat Rev Neurosci* 5(2):97–107.

102. Schweitzer PJ, Fallon BA, Mann JJ, Kumar JS (2010) PET tracers for the peripheral benzodiazepine receptor and uses thereof. *Drug Discov Today* 15(21-22):933–942.

103. Kreisl WC, et al.; Biomarkers Consortium PET Radioligand Project Team (2013) In vivo radioligand binding to translocator protein correlates with severity of Alzheimer's disease. *Brain* 136(Pt 7):2228–2238.

104. Krakauer JW, Pine ZM, Ghilardi MF, Ghez C (2000) Learning of visuomotor transformations for vectorial planning of reaching trajectories. *J Neurosci* 20(23):8916–8924.

105. Huber R, et al. (2006) Arm immobilization causes cortical plastic changes and locally decreases sleep slow wave activity. *Nat Neurosci* 9(9):1169–1176.

106. Shannon BJ, et al. (2013) Morning-evening variation in human brain metabolism and memory circuits. *J Neurophysiol* 109(5):1444–1456.

107. Raichle ME, Martin WR, Herscovitch P, Mintun MA, Markham J (1983) Brain blood flow measured with intravenous H2(15)O. II. Implementation and validation. *J Nucl Med* 24(9):790–798.

108. Videen TO, Perlmutter JS, Herscovitch P, Raichle ME (1987) Brain blood volume, flow, and oxygen utilization measured with 15O radiotracers and positron emission tomography: Revised metabolic computations. *J Cereb Blood Flow Metab* 7(4):513–516.

109. Martin WR, Powers WJ, Raichle ME (1987) Cerebral blood volume measured with inhaled C15O and positron emission tomography. *J Cereb Blood Flow Metab* 7(4):421–426.

110. Mintun MA, Raichle ME, Martin WR, Herscovitch P (1984) Brain oxygen utilization measured with O-15 radiotracers and positron emission tomography. *J Nucl Med* 25(2):177–187.

111. Patlak CS, Blasberg RG (1985) Graphical evaluation of blood-to-brain transfer constants from multiple-time uptake data: Generalizations. *J Cereb Blood Flow Metab* 5(4):584–590.

112. Patlak CS, Blasberg RG, Fenstermacher JD (1983) Graphical evaluation of blood-to-brain transfer constants from multiple-time uptake data. *J Cereb Blood Flow Metab* 3(1):1–7.

113. Shulman GL, et al. (2010) Right hemisphere dominance during spatial selective attention and target detection occurs outside the dorsal frontoparietal network. *J Neurosci* 30(10):3640–3651.

114. Fox MD, Zhang D, Snyder AZ, Raichle ME (2009) The global signal and observed anticorrelated resting state brain networks. *J Neurophysiol* 101(6):3270–3283.

115. Power JD, Barnes KA, Snyder AZ, Schlaggar BL, Petersen SE (2013) Steps toward optimizing motion artifact removal in functional connectivity MRI: A reply to Carp. *Neuroimage* 76:439–441.

116. Power JD, Barnes KA, Snyder AZ, Schlaggar BL, Petersen SE (2012) Spurious but systematic correlations in functional connectivity MRI networks arise from subject motion. *Neuroimage* 59(3):2142–2154.

117. Hayasaka S, Nichols TE (2004) Combining voxel intensity and cluster extent with permutation test framework. *Neuroimage* 23(1):54–63.

118. Behrens TE, et al. (2003) Characterization and propagation of uncertainty in diffusion-weighted MR imaging. *Magn Reson Med* 50(5):1077–1088.

119. Yarkoni T (2009) Big correlations in little studies: Inflated fMRI correlations reflect low statistical power—Commentary on Vul et al. (2009). *Perspect Psychol Sci* 4(3):294–298.

Shannon et al.